Multi-scale Impacts of Variable Heating in Climate

Prashant D. Sardeshmukh and Philip Sura

Climate Diagnostics Center
CIRES, University of Colorado
and Earth System Research Laboratory, NOAA
Boulder, Colorado

Journal of Climate

March 2006

Abstract

While it is obvious that the mean diabatic forcing of the atmosphere is crucial for maintaining the mean climate, the importance of diabatic forcing *fluctuations* is less evident in this regard. Such fluctuations do not appear directly in the equations of the mean climate, but affect the mean indirectly through their effects on the time-mean transient-eddy fluxes of heat, momentum, and moisture. How large are these effects? What are the effects of tropical phenomena associated with substantial heating variations such as ENSO and the MJO? To what extent do variations of the extratropical surface heat fluxes and precipitation affect the mean climate? What are the effects of the rapid "stochastic" components of heating fluctuations? Most current climate models misrepresent ENSO and the MJO and ignore stochastic forcing; they therefore also misrepresent their mean effects. To what extent does this contribute to climate model biases, and to projections of climate change?

This paper provides an overall assessment of such impacts by comparing with observations a long simulation of the northern winter climate by a dry adiabatic general circulation model forced only with the observed time-mean diabatic forcing as a constant forcing. Remarkably, despite the total neglect of all forcing variations, the model reproduces most features of the observed circulation variability and the mean climate, with biases similar to those of some state-of-the-art general circulation models. In particular, the spatial structures associated with the circulation variability are remarkably well reproduced. Their amplitudes, however, are progressively underestimated from the synoptic to the subseasonal to interannual and longer time scales. This underestimation is attributed to the neglect of the variable forcing. The model also excites significant tropical variability from the extratropics on internnual scales, which is overwhelmed in reality by the response to tropical heating variability. The deficiencies of this constant-forcing simulation suggest a substantial role for coherent as well as stochastic transient diabatic forcing in the dynamics of climate variability on different time scales and the mean climate. The results also have implications for identifying priorities in model development at climate modeling centers.

1. Introduction

Despite significant improvements in climate models over the last two decades, the substantial remaining errors in simulations of both the mean climate and climate variability have proved difficult to eradicate. There is evidently a connection between these two types of error, but attempts at a systematic diagnosis quickly run up against the chicken-or-egg issue of whether the errors in the mean cause those in the variability or vice versa. The elegant theory of adiabatic transient-eddy/mean-flow interactions developed over the last several decades is generally unhelpful in this regard, and has also limited applicability to finite amplitude variations in zonally asymmetric environments and to diabatically driven flows in the troposphere. Furthermore, there is no reason why GCMs should not be able to handle such adiabatic interactions, other than inadequate model resolution. The fact that many GCM simulation errors are not qualitatively sensitive to further increases of model resolution suggests that the mishandling of such interactions is not the chief culprit. The pointer thus turns towards the misrepresentation of diabatic processes, as manifested in errors of both the mean and transient diabatic heating.

To some extent, a GCM's mean diabatic heating error can be reduced by the (physical or unphysical) tuning of the GCM's parameterizations. Errors in the variable heating are harder to tune away. Many transient atmospheric phenomena associated with strong heating variations continue to be poorly simulated by GCMs. Prime examples are such tropical phenomena as ENSO and the MJO that dominate on the interannual and intraseasonal time scales; others are not hard to find. It is also relevant in this context that currently there is almost no explicit accounting in GCMs of the "unparameterized remainder" of feedbacks from the unresolved to resolved scales at each model time step. Several modeling groups are exploring ways to treat such feedbacks as additional stochastic forcing terms, but without clear guidance as to their potential impact on climate variability and the mean climate.

Our principal aim in this paper is to provide an overall assessment of how diabatic heating variability affects atmospheric circulation variability and the mean climate, and by implication, how improving representations of transient diabatic phenomena and stochastic forcing in climate models would improve simulations of climate variability and the mean climate. We discuss in Section 2 how the transient forcing does not affect the mean climate directly but indirectly through its effect on the mean adiabatic transient eddy fluxes, and how its overall effect can be assessed - with some limitations - through model simulations in which it is ignored. To this end,

we present in section 3 results from a long 108000-day perpetual winter simulation by a dry adiabatic general circulation model forced with the observed time-mean diabatic forcing as a constant forcing. The errors of this simulation are attributed to the neglect of the transient forcing. Section 4 addresses potential difficulties with such an attribution, and a discussion and concluding remarks follow in section 5.

2. Conceptual Framework

Consider the atmospheric evolution equations in the form

$$\frac{dx_i}{dt} = L_{ij}x_j + N_{ijk}x_j x_k + F_i \tag{1}$$

where x_i is the ith component of the state vector **x**, the first and second terms on the right are the linear and quadratically nonlinear adiabatic tendencies (in which we include linear and quadratically nonlinear damping terms), and all other tendencies are represented by the forcing F_i. For convenience we use throughout this paper the Einstein summation convention of summing over repeated indices; thus $L_{ij}x_j$ actually stands for $\Sigma_j L_{ij}x_j$, etc. Note that L_{ij} and N_{ijk} are constant in time. Now if we write x_i as a sum of mean and transient parts, $x_i = \overline{x}_i + x_i'$, the equation for the mean is

$$\begin{aligned} \frac{d\overline{x}_i}{dt} = 0 &= L_{ij}\overline{x}_j + N_{ijk}\overline{x}_j\overline{x}_k + \underbrace{N_{ijk}\overline{x_j'x_k'}} + \overline{F}_i \\ &= L_{ij}\overline{x}_j + N_{ijk}\overline{x}_j\overline{x}_k + \quad \overline{T}_i \quad + \overline{F}_i \end{aligned} \tag{2}$$

and the equation for the transients, obtained by subtracting (2) from (1), is

$$\begin{aligned} \frac{dx_i'}{dt} &= \underbrace{(L_{ij} + N_{ijk}\overline{x}_k + N_{ikj}\overline{x}_k)x_j'} + \underbrace{N_{ijk}x_j'x_k' - N_{ijk}\overline{x_j'x_k'}} \quad + F_i' \\ &= \qquad M_{ij}x_j' \qquad + \qquad T_i' \qquad + F_i' \end{aligned} \tag{3}$$

where M represents linearization about the mean state and T' the transient adiabatic fluxes. The equation for the eddy covariances $C_{ij} = \overline{x_i' x_j'}$ may then be obtained from (3) as

$$\frac{dC_{ij}}{dt} = 0 = M_{ik}C_{kj} + C_{ik}M_{jk} + \underbrace{\left\{\overline{(T_i' + F_i')x'}_j + \overline{(T_j' + F_j')x_i'}\right\}}_{Q_{ij}} \qquad (4)$$

This equation relates C to the third-order moments $\overline{T'x'}$ and the covariance of F' with x'. Note that one can write an equation like (4) in any norm, i.e. for any linear transformation of x'. In the energy norm C_{ii} is the energy, and $\overline{F_i x_i}$ is the energy source. The impact of the transient forcing F' on the mean climate can thus be seen as occurring through its impact on C (and therefore on $\overline{T}_i$, since $\overline{T}_i = N_{ijk}C_{jk}$) in (4), and then through $\overline{T}_i$ in (2).

Equations (2) and (4) provide a convenient conceptual framework for investigating the interaction between climate variability and the mean climate, and how it is affected by the mean and variable diabatic forcing. A significant simplification occurs if the terms Q_{ij} within the curly brackets in (4) are expressible in terms of $\overline{x}_i$ and C_{ij} plus external sources; then (2) and (4) form a closed set for $\overline{x}_i$ and C_{ij} and there is no need to explicitly consider (3). One simple way to do this (among others) is to approximate $T_i' + F_i'$ in (3) as stochastic forcing terms $S_{im}\eta_m$, where η_m is delta-correlated white noise. The terms within the curly brackets in (4) then become $Q_{ij} = S_{im}S_{jm}$, and (2) and (4) reduce to perhaps the simplest possible closed set of coupled equations linking the mean climate and climate variability. Note that in this case (4) is a linear equation for C, and a stationary positive-definite solution exists only if M is a stable linear operator.

Although no one to our knowledge has attempted to solve such a coupled set of equations, much has been learned by analyzing (2) and (4) separately. There is a long history of studies considering simplified forms of (2) to understand the effects of $\overline{F}$ and $\overline{T}$ on the mean climate $\overline{x}$. A few studies have also used simplified forms of (4) to understand how C is influenced by $\overline{x}$ through M. For example, Whitaker and Sardeshmukh (1998) solved (4) for the C of the extratropical synoptic eddies, specifying an M corresponding to linearization about the observed

long-term mean tropospheric circulation, and also specifying $Q_{ij} = S_{im}S_{jm}$, and obtained remarkably realistic stormtracks. Two aspects of their successful simulation are especially relevant here, as will become evident in the following pages: 1) their model was sufficiently damped that M was stable, as required; and 2) in order to obtain realistic stormtrack magnitudes over the entire northern hemisphere, they adjusted the overall magnitude of their Q_{ij} terms with a single global factor. Thus their success was partly due to their implicitly accounting for the contribution of the F' terms in (4), albeit in a crude manner.

We are concerned in this paper with the effect of F' not just on C but also on the mean $\bar{x}$, and a consistent treatment requires that we consider (2) and (4) together. We recognize that while the $Q_{ij} = S_{im}S_{jm}$ approximation is illuminating, it may not be accurate enough for a quantitatively useful diagnosis of a GCM's erroneous simulated mean and variability. Such a closure of Q, or indeed any closure at all, is in fact unnecessary in (4) if we consider (3) explicitly, i.e. if we run the model (1) with prescribed mean and variable forcings. To generate the long simulation described in the next section, we forced a dry adiabatic GCM with only the mean observed forcing, and interpreted the errors in its simulated mean and variability as arising from the neglect of the variable forcing F'. Despite some potential difficulties with this interpretation discussed later in the paper, we are confident that the errors of our constant-forcing simulation do provide useful estimates of the net impacts of diabatic heating variability on atmospheric circulation variability and the mean climate.

3. A Constant-Forcing Simulation

To assess the net impacts of diabatic forcing variability in climate, we performed a long 108000-day perpetual winter integration of a dry adiabatic GCM forced with the observed winter-mean diabatic forcing as a constant forcing. For this purpose we used a T42 5-level version of the University of Hamburg's Portable University Model of the Atmosphere (PUMA), which may be downloaded from http://www.mi.uni-hamburg.de/Theoretische_Meteorologie.6.0.html. The model incorporates simple parameterizations of thermal and mechanical damping similar to those used by Hoskins and Simmons (1975) and Hall (2000). Specifically, a horizontal ∇^8 hyperdiffusion with a timescale of 6 h at the smallest resolved scale is included in the equations for vorticity, divergence, and temperature. An additional scale-independent but level-dependent linear damping is also imposed on these variables. For vorticity and divergence this linear

damping is strongest (1 day) at the lowest model level (σ=0.9) and much weaker (30 days) at higher levels. Similarly for temperature, the linear damping is strongest at the lower levels (1 day at σ=0.9 and 5 days at σ=0.7) and much weaker (30 days) at higher levels. The time-integration scheme is a filtered leap-frog scheme (Asselin 1972) with a timestep of 30 minutes and the filter parameter set to 0.02.

We estimated the observed mean $\overline{F}$ as the (sign-reversed) average initial tendency of the *unforced* adiabatic model (1) initialized by the daily-averaged 6-hourly wintertime NCEP/NCAR observational reanalyses of 1970-1999, removing the small long-term observed tendency associated with the 30-year trend. (The NCEP dataset used was actually a "chi-corrected" version generated by us by modifying the 6-hourly wind divergence fields to balance the large-scale vorticity and mass budgets (Sardeshmukh 1993; Sardeshmukh et al 1999). The particular advantage of using such a corrected dataset is that there are no spurious vorticity or mass sources in the diagnosed F arising from data analysis errors in the horizontal wind divergence fields). A similar procedure was followed by Hall (2000) with a T21 5-level model like ours, and by Lin and Derome (1996), Marshall and Molteni (1993), and Roads (1987) with T21 3-level and 2-level quasi-geostrophic models. All of these investigators used much shorter observational records than us to estimate $\overline{F}$. All, like us here, then integrated their models with $\overline{F}$, but for different purposes and for much shorter periods than our 108 000 day run. The study of Hall (2000) was closest to ours, and our results are generally consistent with his results.

In this section, we present some basic comparisons of our constant-forcing simulation with observations to provide a flavor of its realism and deficiencies. We begin with hemispheric 1-point correlation maps (also known as 1-point teleconnection maps, see Wallace and Gutzler 1981) with respect to base points in the North Pacific and North Atlantic regions of the strongest observed synoptic and low-frequency variability, follow up with hemispheric maps of geopotential height variance and momentum and heat fluxes, then with latitude-height cross sections of the zonal means of these quantities, and end with a comparison of the simulated and observed mean climates.

3.1 *One-point correlation maps of 500 mb height variability*

To facilitate comparisons of the simulated and observed variability on different time scales, we filtered the 500 mb height daily time series at each grid point using a 21-point Lanczos filter

(Duchon 1979) to isolate variations with periods between 2 and 6 days (the "synoptic" band), greater than 10 days (the "low-frequency" band), between 10 and 90 days (the "intraseasonal" band), and greater than 180 days (the "interannual" band). As a further check on the robustness of our surprising "interannual" band results, we also compared the variability of the simulated 90-day averages with that of observed 90-day averages.

Figure 1 compares the simulated (left) and observed (right) correlations of 500 mb height variations in the synoptic band for base points in the north Pacific and north Atlantic regions of strongest observed synoptic variability. Note that to enable a cleaner comparison of the simulated and observed correlations in these and all other such maps to follow, the base points in the simulation plots were chosen to be identical to those in the observational plots. These base points may be identified on the plots as the points at which the correlation is unity. To save space, Figure 1 also combines the two separate correlation patterns obtained for the Pacific and Atlantic base points into a single map, as the geographical overlap of the separate patterns is negligible.

Given the vast simplicity of our model vis-à-vis state-of-the-art GCMs, plus the neglect of *all* variable forcing, the general agreement of the simulated and observed synoptic-eddy correlations in Figure 1 must be regarded as remarkable. Consistent with numerous previous studies, this confirms that to a first approximation the dynamics of extratropical synoptic variability are adiabatic. Closer comparison of the simulated and observed panels, however, reveals significant local discrepancies. To what extent these are primarily due to model deficiencies or the neglect of the transient forcing is unclear at present. It is also interesting that the statistically significant impact of ENSO on winter-mean stormtracks documented by Sardeshmukh et al (2000), Compo et al (2001), Compo and Sardeshmukh (2004) and others, which contributes to the observed but not the simulated panels in Figure 1, is minor in terms of this statistic. From the equatorward (poleward) shift of the tail-end of the Pacific stormtrack during El Nino (La Nina), one would expect the observational correlation contours to be slightly more meridionally elongated and bow-shaped in the eastern Pacific basin compared to the model contours, but the effect is very slight.

Figure 2 shows the observed and simulated 1-point correlations of the low-frequency (> 10 day) 500 mb height variations with those at base points in the North Atlantic (upper panels) and North Pacific (lower panels) basins. For the North Atlantic base point, the agreement between the simulated and observed correlations is almost as good as in Figure 1, but for the North Pacific base point it is not. The simplest interpretation of this is that the neglected transient forcing has a

relatively large impact in the tropics and the Pacific-North American (PNA) sector, but not in the region of the North-Atlantic oscillation (NAO). The former is not surprising given our neglect of all tropical diabatic forcing variations associated with the MJO and ENSO that have large impacts in the tropics and the PNA sector. The relatively minor impact of the transient forcing on the spatial structure of NAO variability is, however, a surprise with implications for the effect of north Atlantic SST variations on the NAO .

To clarify the impacts of transient forcing on the spatial structures of intraseasonal (10-90 day) and lower frequency (> 180 day) circulation variability, Figures 3 and 4 present the 1-point correlations of variations on these time scales in an identical format to that of Figure 2. (Note again that the base points in these and all such figures in this paper were chosen to correspond to those with the largest observed variability in the Pacific and Atlantic basins in their respective frequency bands). In Figure 3, the simulated intraseasonal correlations again match well with those observed in the Atlantic sector. More surprisingly, they also match much better in the Pacific sector than in Figure 2; the main difference being that the simulated lobe of negative correlations upstream of the base point is shifted farther west into China compared to its position over Kamachatka in the observations. If we attribute this difference to the neglect of MJO heating, then the lower panels of Figure 3 suggest that the MJO significantly affects the spatial structure of subseasonal variability over east Asia and the northwest Pacific.

Figure 4 presents the 1-point correlations of the interannual and longer-term 500 mb height variations with periods greater than 180 days. The simulated and observed correlation patterns are again very similar for the North Atlantic base point. For the Pacifc base point, they are also similar in the middle and high latitudes, but radically different – even in sign – in the tropics and subtropics. The observed negative tropical correlations are consistent with ENSO variability, but the simulated correlations - without ENSO variability - are also equally large throughout the tropics, and positive. This is a major surprise. To confirm that the discrepancy is not somehow an artifact of our frequency filter, Figure 5 shows, in an identical format to Figure 4, the 1-point correlation maps for 90-day average 500 mb height variations with respect to the North Pacific base point. The result is very similar to that in the lower panels of Figure 4. The simulated correlation maps for the height variations at other vertical levels (not shown) are also similar. The positive tropical correlations are in fact strongest (>0.6) at 300 mb and decrease above and below that level; they are nearly zero at 700 mb and slightly negative at 900 mb.

Since there is no transient forcing in our model, there is no mechanism to generate tropical variability except by extratropical excitation. Consistent with this, Figure 6 shows that the running 90-day averages of tropically averaged (20N-20S) 500 mb heights lag the running 90-day averages of 500 mb heights at the North Pacific base point by about 10 days. The smaller tropical correlations from 300 mb downward are also consistent with excitation from the jet level in midlatitudes.

In summary, Figures 1 through 4 contain two surprises. The first is the suggestion that transient diabatic forcing has only a minor impact on the spatial structures of northern hemispheric circulation variability. The second is that on interannual and longer scales, extratropical variability can excite significant spatially coherent geopotential height variability in the tropics.

We hasten to add that while the effects of the transient forcing on the *spatial structures* of extratropical circulation variability are minor, the effects on their *magnitudes* are not. Table 1 summarizes the standard deviations of the observed and simulated 500 mb height variations in the different frequency bands, at our selected North Atlantic and North Pacific base points as well as averaged over the hemisphere poleward of 20N. The magnitude of the variability is consistently underestimated in our constant forcing simulation, with the underestimate being relatively minor (10% or less) on the synoptic scale and worsening to as much as 50% on the interannual and longer scales.

3.2 *Hemispheric maps of variances and fluxes*

Figure 7 compares three different aspects of the simulated daily variability with observations: the mean transient-eddy poleward zonal momentum flux in the upper troposphere (upper panels), the mean transient-eddy poleward temperature flux in the lower troposphere (middle panels), and the standard deviation of daily 500 mb heights (lower panels). Consistent with the results of the previous subsection, the geographical distributions of all three quantities are reasonably well simulated, but their magnitudes are underestimated. The momentum fluxes are somewhat stronger than observed (except over North Africa), whereas the heat fluxes and height variability are clearly weaker.

3.3 *Zonal mean fluxes and variability*

Figure 8 shows that the meridional and vertical variations of the zonally averaged poleward fluxes of zonal momentum and temperature, as well as the zonally averaged standard deviations of geopotential heights, are also well simulated. The principal deficiencies are a generally weaker height variability than observed, except in the polar stratosphere where it is stronger; weaker lower-tropospheric temperature fluxes above the boundary layer in mid-latitudes, and momentum fluxes of the wrong sign in high latitudes.

From equation (4), one expects the neglect of transient forcing to lead to an overall reduction of eddy kinetic energy. The left panel of Figure 9 compares the vertical profiles of the simulated and observed transient eddy kinetic energy (EKE) averaged over the hemisphere poleward of 20N. Consistent with the lower panels of Figures 7 and 8, the simulated EKE is indeed significantly weaker than observed. It is interesting that a similar error also occurs in the state-of-the-art NASA GCMs with much higher vertical resolution, documented by Robinson and Black (2005) and reproduced here in the right panel of Figure 9. One wonders to what extent it is also due to weak transient diabatic forcing in those GCMs.

3.4 *Time-mean maps*

Finally, Figure 10 compares the simulated and observed long-term mean zonally asymmetric fields of 500 mb heights. The observational averages are over the same 30 winters used for calculating $\overline{F}$; the model averages are over the 108000 simulated days. The agreement is generally excellent, except that the model's ridge over western Canada is too strong. Given our neglect of *all* transient diabatic forcing and the model's obvious deficiencies (especially its crude vertical resolution), it would indeed be astonishing if the agreement were much better. Nonetheless, it is noteworthy that a similar error over western Canada, and of a similar magnitude, occurs in a 34-level NASA/NSIPP GCM simulation with prescribed SSTs for 1979-96 (Robinson and Black 2005; see their Figure 1).

We have visually compared these and other aspects of our simulation with those of other GCMs in the published literature. Our mean biases appear to be well within the range of biases of GCMs participating in the AMIP project (Gates et al 1999). For various reasons, documentations of even basic measures of GCM-simulated circulation variability such as shown here are not as yet widely

available; possibly because regular archival of the voluminous daily output from long GCM runs is a relatively recent practice. It would certainly be interesting to assess to what extent, if any, the current generation of atmospheric and coupled GCMs are better at reproducing the aspects of observed extratropical circulation variability depicted in Figures 1 through 8 than our simple model with specified observed time-mean forcing.

4. Attribution to Transient Forcing

To what extent can the deficiencies of our constant-forcing simulation be attributed only to our neglect of F'? There can be little doubt that the model's limited T42 5-level resolution and the errors in its simple damping parameterizations also contribute. Is it possible that our relatively weak simulated variability is due to excessive damping,? The fact that the NASA models also show a similar weakness in Fig 9 is reassuring in this regard, but not conclusive, since the damping could be excessive in those (and other) GCMs as well.

Clearly, our model is not so strongly damped that it has no variability; the issue is just whether the damping is stronger than in reality. We do not believe this to be case after performing the following additional simulation with a constant forcing $\overline{F}_{ci} = \overline{F}_i + \overline{T}_{oi}$, where $\overline{T}_{oi}$ is the observed mean transient-eddy flux. This forcing is simply the sign-reversed initial tendency of the unforced model (1) when initialized with the observed mean climatology, with the small tendency of the 30-yr trend removed. In an excessively damped model, such a forcing would maintain a constant model state, i.e the observed mean state, and there would be no variability. In other words, the linear operator M in (3) would be stable, and (4) would have a trivial null solution. The issue thus boils to down to whether the observed mean state is stable or unstable for realistic damping. Hall and Sardeshmukh (1998) examined this matter in some detail, and concluded that the observed mean state was close enough to being neutral that it was "pointless to come down on one side of the fence or the other". As mentioned earlier, Whitaker and Sardeshmukh (1998) simulated realistic storm tracks for damping parameters that rendered M weakly stable. These studies, as well as theories of baroclinic adjustment, suggest that for realistic damping M is neutral or weakly stable. By this logic, we should obtain little or no variability in our $\overline{F}_c$ run if our damping is realistic.

As Figure 11 shows, the variability is indeed considerably weaker in this run than in the $\overline{F}$ run, but is not zero, which suggests that if anything, our damping may be too *weak*, not too strong. We

therefore conclude that despite our model's limitations, our results do indicate a substantial role for diabatic forcing variations in influencing not only climate variability but also the mean climate.

Another potential concern with our diagnosis is the decoupling of the forcing and the circulation, i.e the specification of diabatic heating as an "external" forcing. Similar concerns also arise when diagnosing any subsystem of the complete coupled climate system with a subsystem model, and representing all other influences as external or boundary forcing. This is not a black-or-white issue but one with varying shades of gray, depending on the problem at hand. For example, despite the obvious coupling of the atmosphere and the ocean, a great deal has been learned about their dynamics and variability using atmospheric and oceanic GCMs with prescribed SST and surface wind stress and heat flux "forcings", respectively. The decoupling issue becomes relatively more important when a mechanical or thermal damping mechanism is mis-specified as a "forcing" F'; this can alter the sign of $\overline{F'x'}$ in (4) and introduce spurious energy sources and sinks in the system. We do not believe the forcing-circulation decoupling to be a serious concern here partly because we do not have F' in our constant-forcing simulation. The underestimation of the eddy kinetic energy in Figure 9 also clearly suggests the need for an additional energy source, i.e. a forcing, not an energy sink.

5. Discussion and Concluding Remarks

The deficiencies of our constant-forcing simulation indicate a substantial role for transient diabatic forcing in the dynamics of circulation variability on different time scales and the mean climate. Given the relatively low resolution of our model and its simple representations of mechanical and thermal damping, a precise quantification of this role is difficult, but the general conclusion is clear. An obvious next step would be to repeat such constant-forcing simulations with higher resolution dry adiabatic GCMs with more sophisticated treatments of mechanical and thermal damping. This is a topic of current research.

What particular aspects of the variable forcing, in what geographical regions, and on what time scales, are relatively more important ? We have not addressed this issue in any detail, although Table I is certainly consistent with numerous studies showing the impact of MJO heating on intraseasonal variability and of ENSO on interannual variability A more quantitative assessment could be made by adding various components of the transient forcing to the constant forcing in

our nonlinear dry adiabatic GCM, and assessing their impacts on the simulated variability and the mean climate. This too is a topic of current research. Previous studies have mostly investigated such impacts in linear models, not in nonlinear models that simulate transient eddies and allow for nonlinear transient-eddy / mean-flow interactions.

The remarkable similarity of the simulated and observed correlation patterns in Figures 1 and 3 also suggests a substantial role for stochastic diabatic forcing in the dynamics of synoptic and subseasonal variability. If forcing structure were important, it would alter the structure of the circulation variability. Indeed we had argued earlier that the *dissimilarity* of the simulated and observed intraseasonal structures in the lower panels of Figure 3 suggest a role for MJO forcing in the Pacific sector. By the same token, the *similarity* of such patterns argues against the importance of forcing structure, i.e suggests a role for stochastic forcing.

The results in Figures 1 and 3 (and the corresponding entries in Table 1) are entirely consistent with the linear stochastically-driven view of synoptic and subseasonal atmospheric variability proposed by Whitaker and Sardeshmukh (1998), Winkler et al (2001), Newman et al (2003), and Newman and Sardeshmukh (2006, forthcoming). The comparison with Whitaker and Sardeshmukh's linear model results is especially illuminating. Their simulated 1-point correlations in the Pacific and Atlantic stormtrack regions were as good as ours, but their model was baroclinically stable, whereas ours (as Figure 11 shows) is not. Our excellent simulation in Figure 1 even in a baroclinically unstable environment therefore suggests not only that the neglected transient diabatic forcing is effectively stochastic on the synoptic scale, but also that the nonlinear T' terms in equation (3) can be approximated as a simple linear damping plus stochastic noise (Farrell and Ioannou 1995, Whitaker and Sardeshmukh 1998, Delsole 2004). Whitaker and Sardeshmukh (1998) augmented the dissipation in their linear model with such a simple (~10-day) damping, thereby stabilizing it, and in effect combined the stochastic noise with the stochastic diabatic forcing in specifying a total stochastic forcing that not only reproduced the spatial structures of the observed synoptic variability but also its amplitude. The competitiveness with GCMs of the stochastically-driven linear inverse model of W inkler et al (2001), Newman et al (2003), and Newman and Sardeshmukh (2006, forthcoming) at simulating and predicting extratropical subseasonal variations is then also understandable. The linear inverse model estimates an effective M operator in equation (3) from observed lag-correlations, and an effective stochastic forcing from a Fluctuation-Dissipation relationship (see e.g. Penland and Matrosova 1994, Penland and Sardeshmukh 1995). Such a linear model would not be competitive with

comprehensive GCMs unless the *T'* terms could be approximated as above and a significant fraction of the transient diabatic forcing could be treated as stochastic.

In conclusion, our results suggest a substantial role for both coherent and stochastic diabatic forcing variability in the dynamics of atmospheric circulation variability and the mean climate. These effects span across time scales. For example, the effect on the mean climate occurs through the effect of the transient forcing on the mean transient-eddy momentum and heat fluxes The transient forcing thus not only directly influences the circulation variability on each time scale, but also facilitates interctions across scales through its influence on the adiabatic fluxes. This has implications for improving predictions on all time scales in the climate system.

Acknowledgments

We thank the Hamburg PUMA modeling group and M. Newman for help with the PUMA model. Discussions with our colleagues at the Climate Diagnostics Center, especially M. Newman and C. Penland. are also gratefully acknowledged. This research was partly supported by funding from the Office of Naval Research and the NOAA's Office of Global Programs .

References

Asselin, R., 1972: Frequency filter for time integrations. *Mon. Wea. Rev.*, **100**, 487–490.

Compo, G.P., and P.D. Sardeshmukh, 2004: Storm track predictability on seasonal and decadal scales J. *Climate,* **17**, 3701-3720

Compo, G.P., Sardeshmukh, P.D., and C. Penland, 2001: Changes of subseasonal variability associated with El Niño. *J. Climate*, **14**, 3356-3374.

DelSole, T., 2004: Stochastic models of quasigeostrophic turbulence. *Surv. Geophys.*, **25**, 107–149.

Duchon, C. E., 1979: Lanczos filtering in one and two dimensions. *J. Applied Meteorology*, **18**, 1016-1022.

Farrell, B. F., and P. J. Ioannou, 1995: Stochastic dynamics of the midlatitude atmospheric jet. *J. Atmos. Sci.,* **52**, 1642–1656

Gates, W.L., and coauthors, 1999: An overview of the results of the Atmospheric Model Intercomparison Project (AMIP I) *Bull. Amer. Met. Soc*., 80, 29-55

Hall, N.M.J., 2000: A simple GCM based on dry dynamics and constant forcing. *J. Atmos. Sci.* 56, 1557-1572

Hall, N.M.J., and P. D. Sardeshmukh, 1998: Is the time mean Northern Hemisphere flow baroclinically unstable? *J. Atmos. Sci.* 55, 41-56.

Hoskins, B.J., and A.J. Simmons, 1975: Multilayer spectral model and semi-implicit method. *Quart. J. Royal. Meteorol. Soc*., 101, 637-655

Lin, H., and J. Derome, 1996: Changes in predictability associated with the PNA pattern *Tellus Series A-Dynamic Meteorology and Oceanography*. 48, 553-571

Marshall, J., and F. Molteni, 1993: Toward a dynamical understanding of planetary-scale flow regimes.*J. Atmos. Sci.* 50, 1792-1818

Newman M, Sardeshmukh PD, Winkler CR, and JS Whitaker, 2003: A study of subseasonal predictability. *Mon. Wea. Rev*., **131**, 1715-1732

Penland, C., and L. Matrosova, 1994: A balance condition for stochastic numerical models with application to the El Niño–Southern Oscillation. *J. Climate*., *7, 1352–1372*.

Penland, C., and P. D. Sardeshmukh, 1995: The optimal growth of tropical sea surface temperature anomalies. *J. Climate*., *8, 1999-2024.*

Roads, J.O., 1987: Predictability in the extended range. *J. Atmos. Sci,* 44, 3495-3527

Robinson D.P., and R.X. Black, 2005: The statistics and structure of subseasonal midlatitude variability in NASA GSFC GCMs. *J. Climate*, **18,** 3294-3316

Sardeshmukh, P.D., 1993: The baroclinic chi problem and its application to the diagnosis of atmospheric heating rates. *J. Atmos. Sci, 50, 1099-1112.*

Sardeshmukh, P. D., M. Newman, and C. R. Winkler, 1999: Dynamically consistent estimates of diabatic heating. Proceedings 24th Annual Climate Diagnostics and Prediction Workshop, Tucson, AZ, NOAA, 172–175.

Sardeshmukh, P.D., Compo, G.P., and C. Penland, 2000: Changes of probability associated with El Nino.*J. Climate*, **13**, 4268-4286

Wallace, J. M., and D. S. Gutzler, 1981: Teleconnections in the geopotential height field during the Northern Hemisphere winter. *Mon. Wea. Rev*., **109**, 784–804.

Whitaker, J.S., and P. D. Sardeshmukh, 1998 A linear theory of extratropical synoptic eddy statistics. *J. Atmos. Sci,* **55***, 237-258.*

Winkler, C. R., M. Newman, and P. D. Sardeshmukh, 2001: A linear model of wintertime low-f frequency variability. Part I: Formulation and forecast skill. *J. Climate*, **14**, 4474-4494.

R.M.S of wintertime 500 mb Geopotential Height variations (meters)

Averaged over the northern extratropics (Lat: 20-90 North, Lon: 0-360)

	NCEP	**PUMA (F_bar)**
2-6 days	26.10	25.54
10-90 days	38.61	31.15
> 180 days	63.17	41.32
> 10 days	84.01	59.18

At North-Atlantic base-points

	NCEP	**PUMA (F_bar)**
2-6 days	62.70	61.18
10-90 days	67.20	43.91
> 180 days	113.50	56.61
> 10 days	148.66	82.06

At North-Pacific base-points)

	NCEP	**PUMA (F_bar)**
2-6 days	49.63	44.22
10-90 days	64.23	42.05
> 180 days	116.13	66.87
> 10 days	150.40	90.25

Table 1. Root-mean-square of filtered 500 mb geopotential height variations in the indicated frequency bands averaged over the hemisphere poleward of 20N (top) and at selected points North Atlantic (middle) and North Pacific (bottom) discussed in the text. The observed and simulated values are listed under the "NCEP" and "PUMA(F_bar)" headings, respectively.

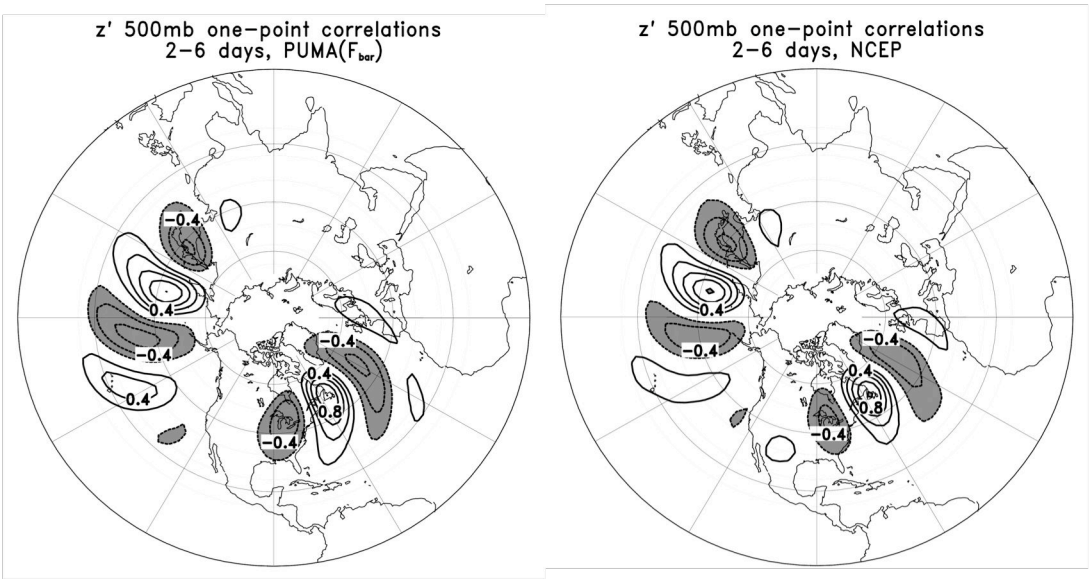

Figure 1. Correlations of 500 mb geopotential height variations in the synoptic (2 to 6 day period) band with those at base points in the northwest Pacific and northwest Atlantic basins in the constant-forcing model simulation (left) and in observations (right). The contour interval is 0.2 and values less than -0.2 are shaded. The zero contour is suppressed.

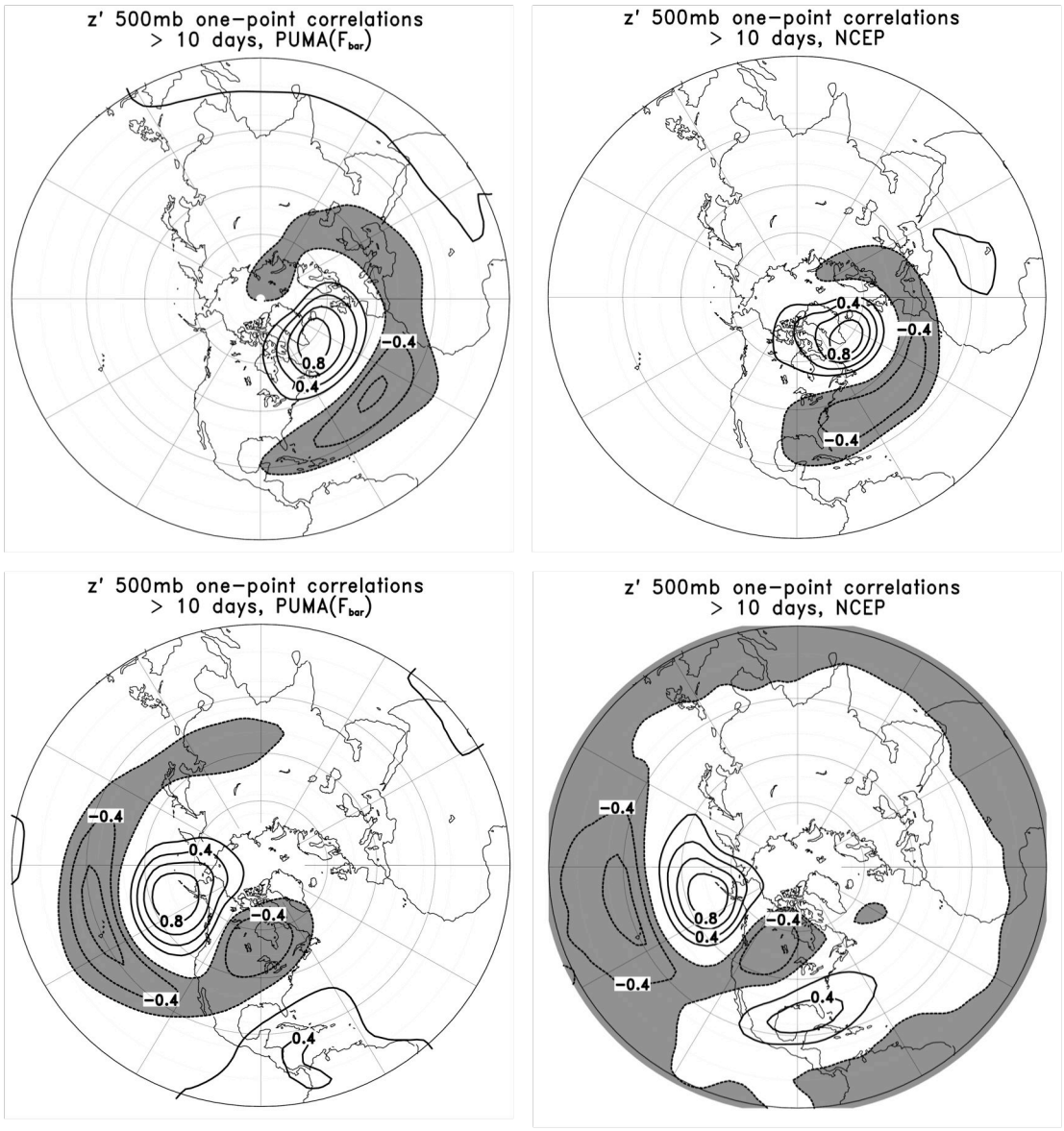

Figure 2. Correlations of low-frequency 500 mb height variations (with periods greater than 10 days) with those at a reference base point in the North Atlantic (upper panels) and in the North Pacific (lower panels) in the constant-forcing simulation (left panels) and in observations (right panels). Contouring as in Figure 1.

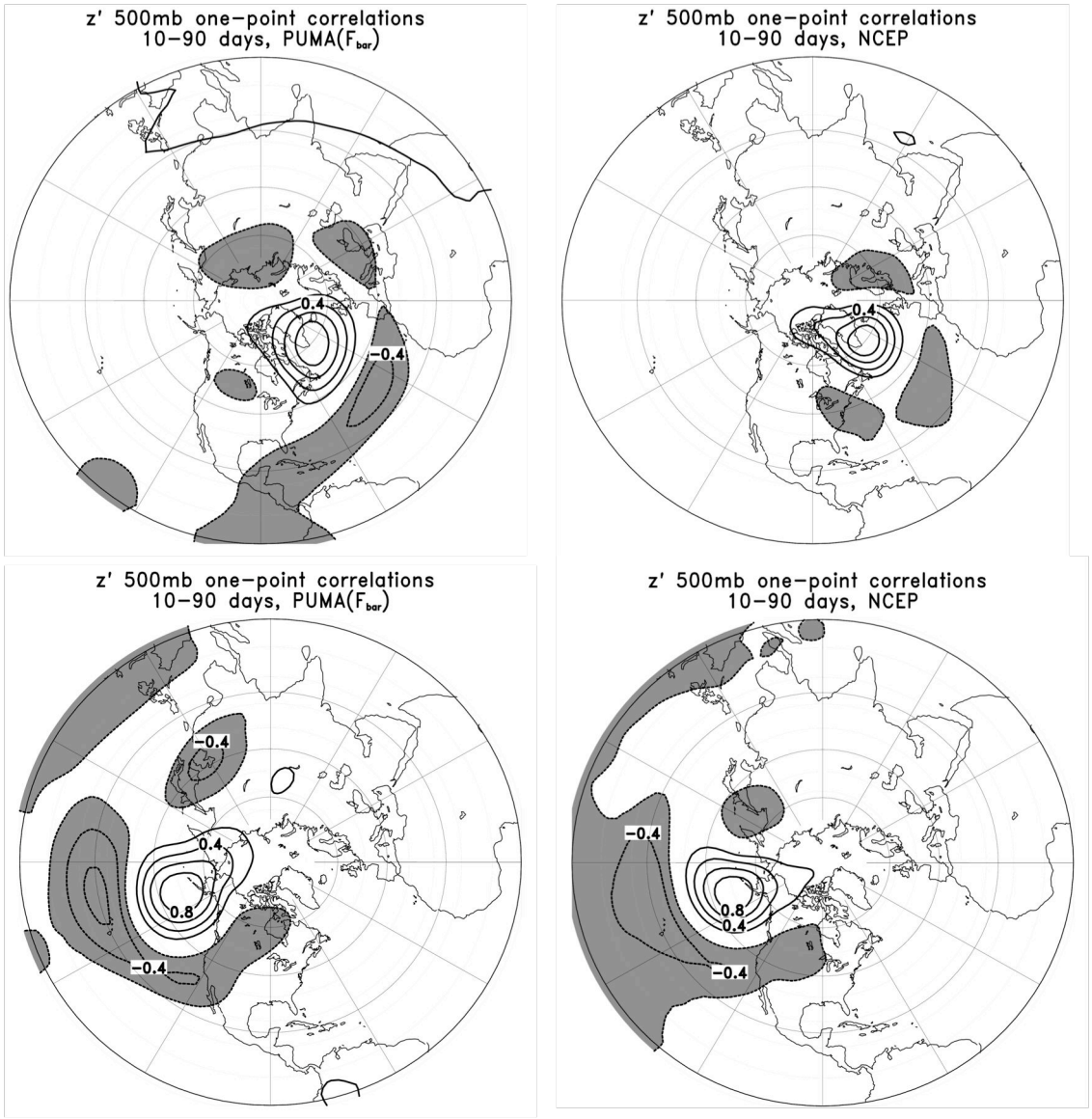

Figure 3. As in Figure 2 but for 500 mb geopotential height variations in the intraseasonal frequency band (with periods between 10 and 90 days).

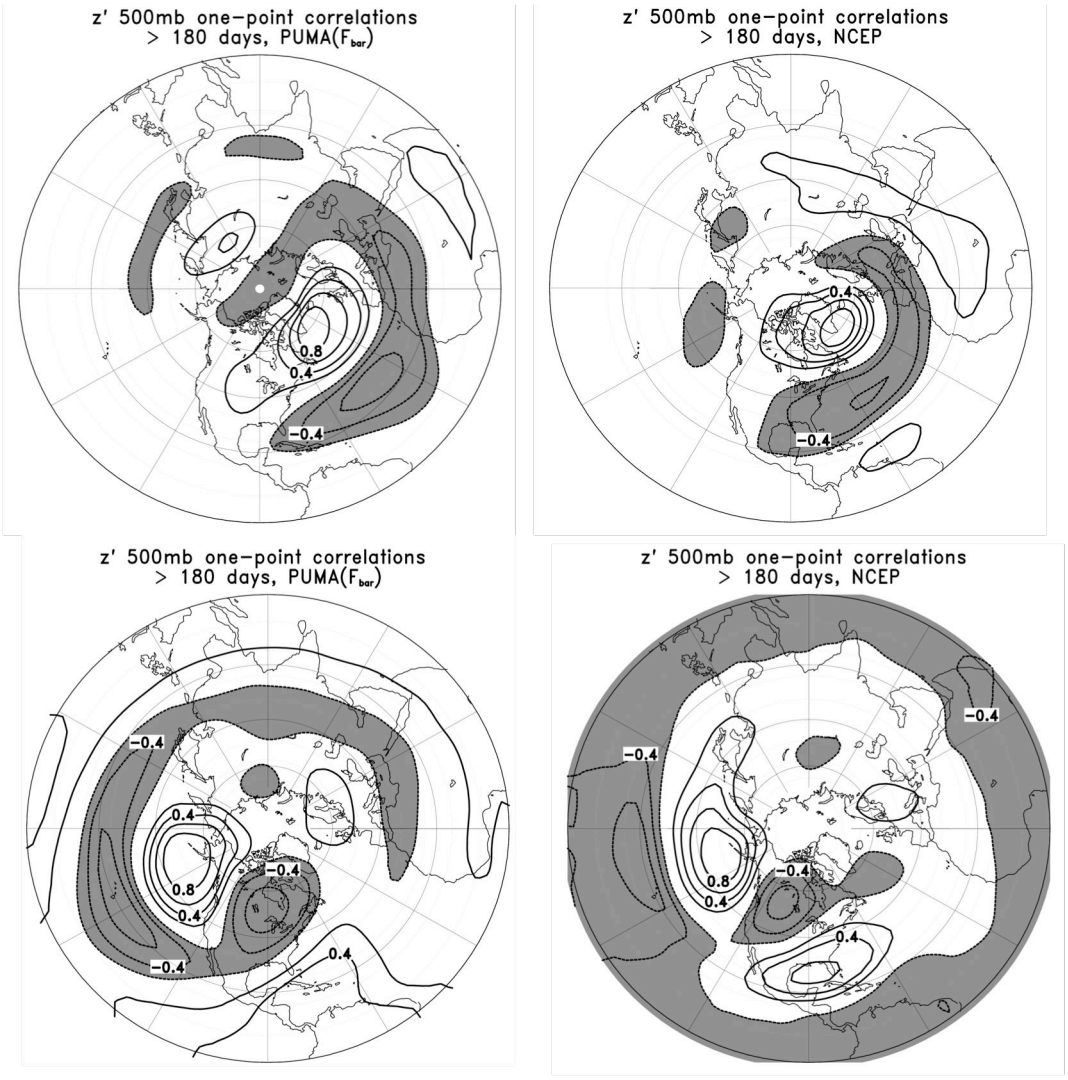

Figure 4. As in Figure 2 but for interannual and longer-term 500 mb height variations (with periods greater than 180 days).

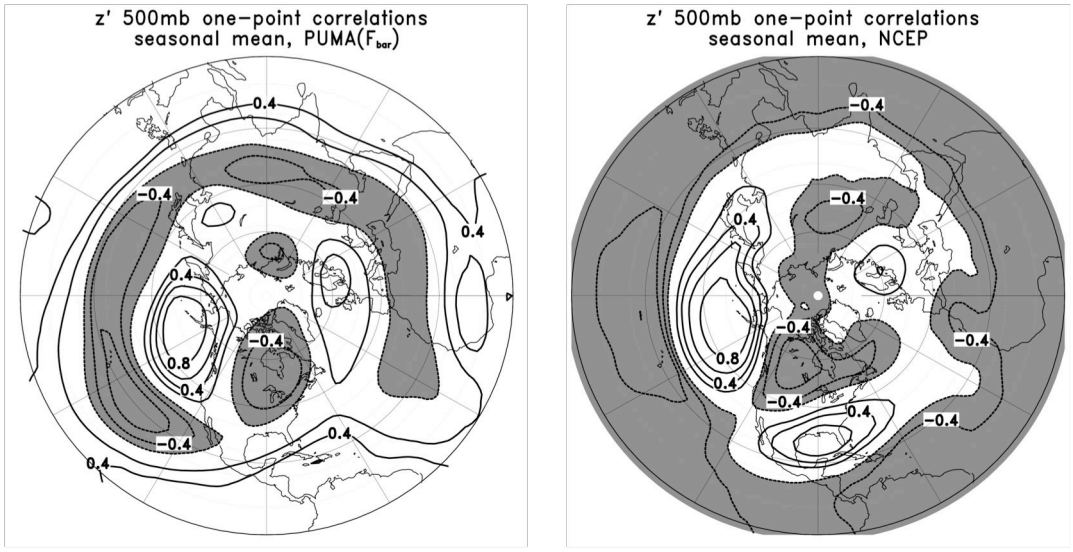

Figure 5. As in Figure 4 but for 90-day average 500 mb height variations.

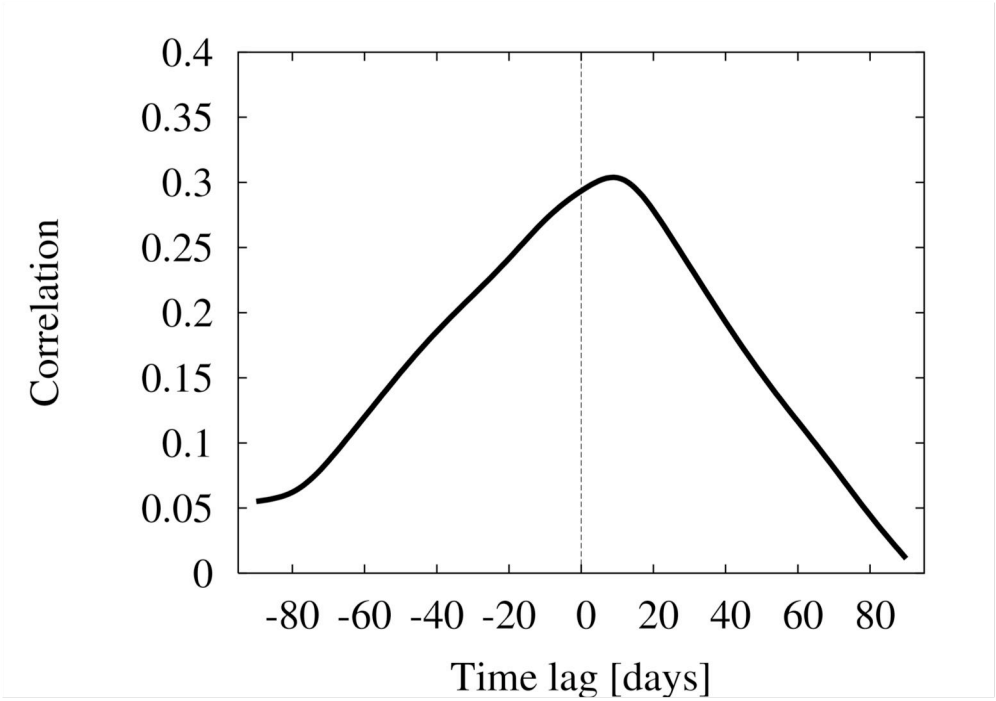

Figure 6. Simulated time-lag correlation of running 90-day average of tropically averaged (20N-20S) 500 mb height variations with running 90-average 500 mb height variations at the North Pacific reference base point used in Figure 5. Positive lag corresponds to the tropical heights lagging the North Pacific heights.

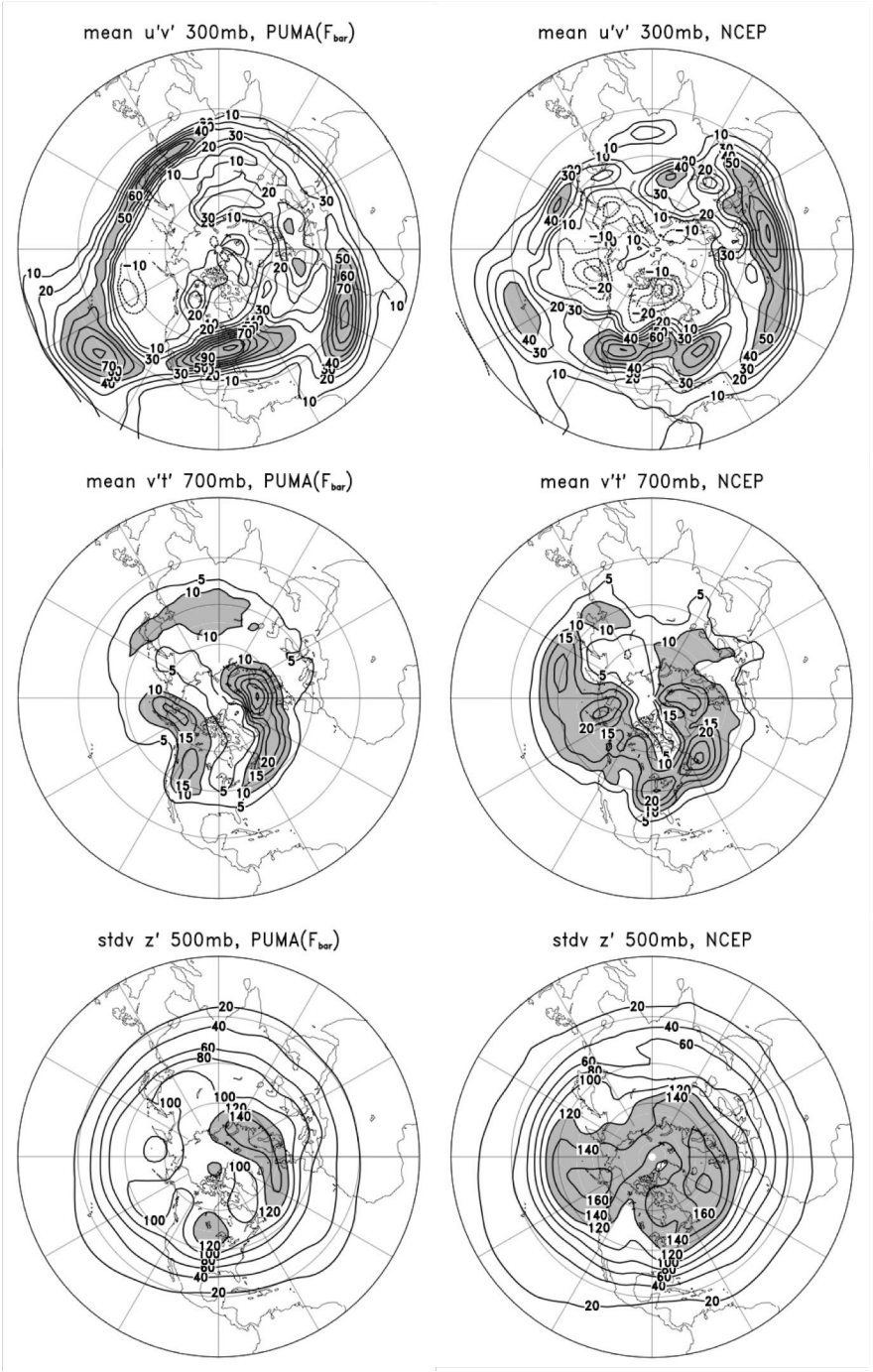

Figure 7. Simulated (left panels) and observed (right panels) statistics of daily variability. Top: mean poleward zonal momentum flux (m^2/s^2) at 300 mb. Middle: mean poleward heat flux (K m/s) at 700 mb. Bottom: standard deviation of 500 mb heights (m). Negative values are dashed. Large positive values are shaded for clarity

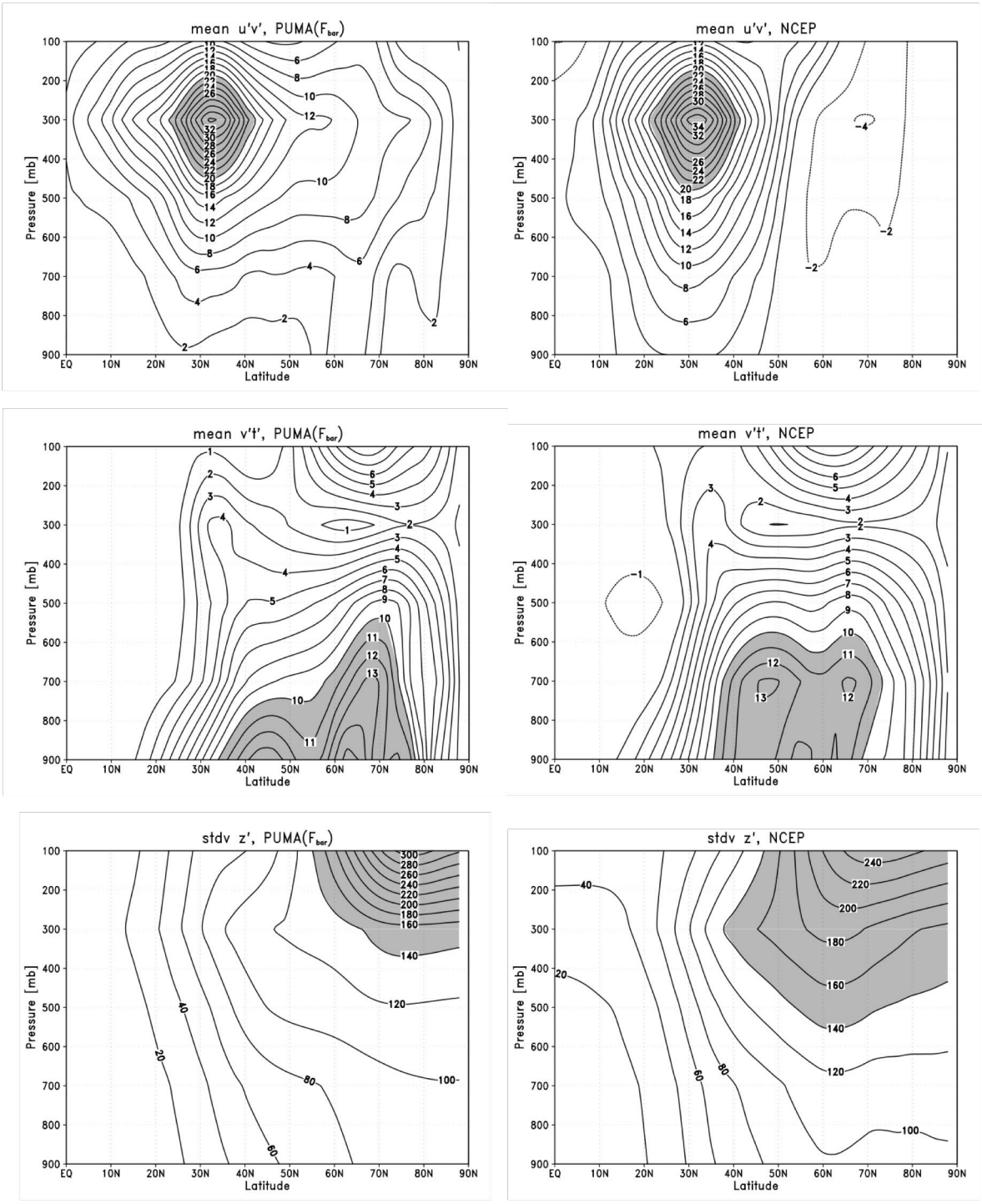

Figure 8. As in Figure 3 but for the latitude and height variation of the zonally averaged poleward momentum flux (top), poleward heat flux (middle) and standard deviation of geopotential heights (bottom) of the simulated (left panels) and observed (right panels) daily variability. Large positive values are shaded for clarity. Negative values are dashed. The zero contour is not shown.

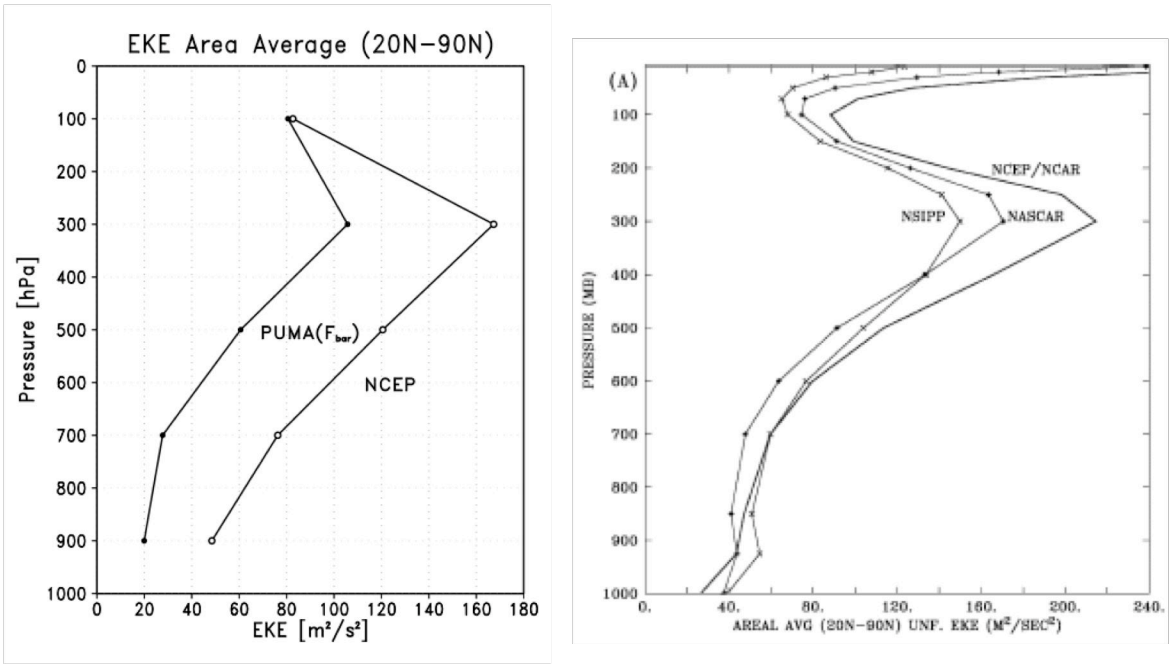

Figure 9. Left panel: Vertical profiles of simulated and observed eddy kinetic energy (EKE) averaged over the northern extratropics (20N-90N). Right panel: A similar plot adapted from Robinson and Black (2005) of the observed EKE for 1979-96 and for two NASA GCM simulations of that period with prescribed observed SSTs.

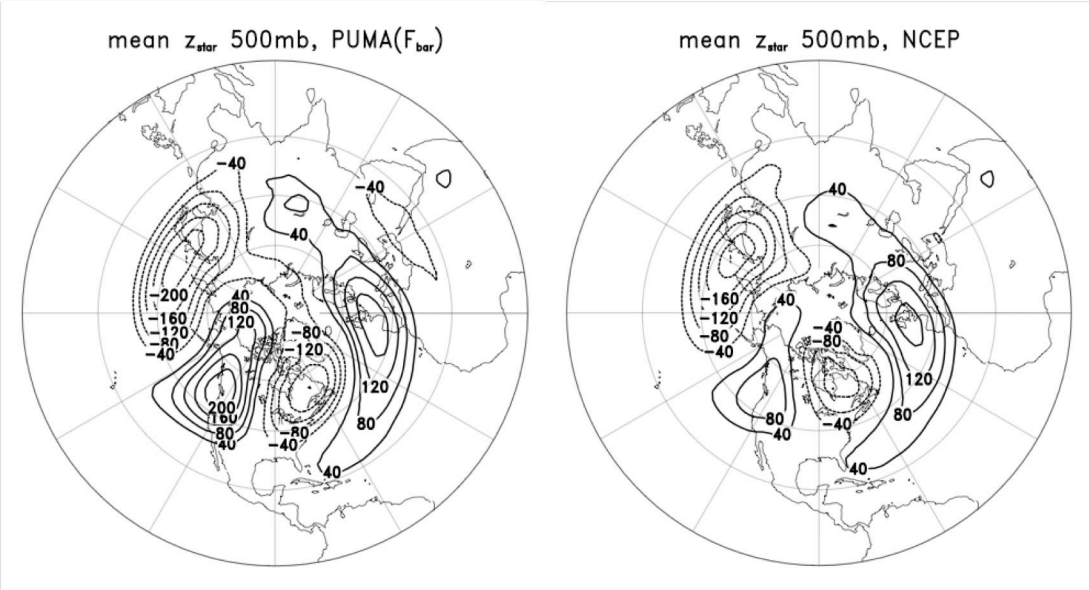

Figure 10. The wintertime (DJF) long-term mean zonally asymmetric 500 mb geopotential height field in the constant forcing simulation (left panel) and in the NCEP/NCAR reanalyses (right panel). The contour interval is 40 m, and negative values are dashed. The zero contour is not shown.

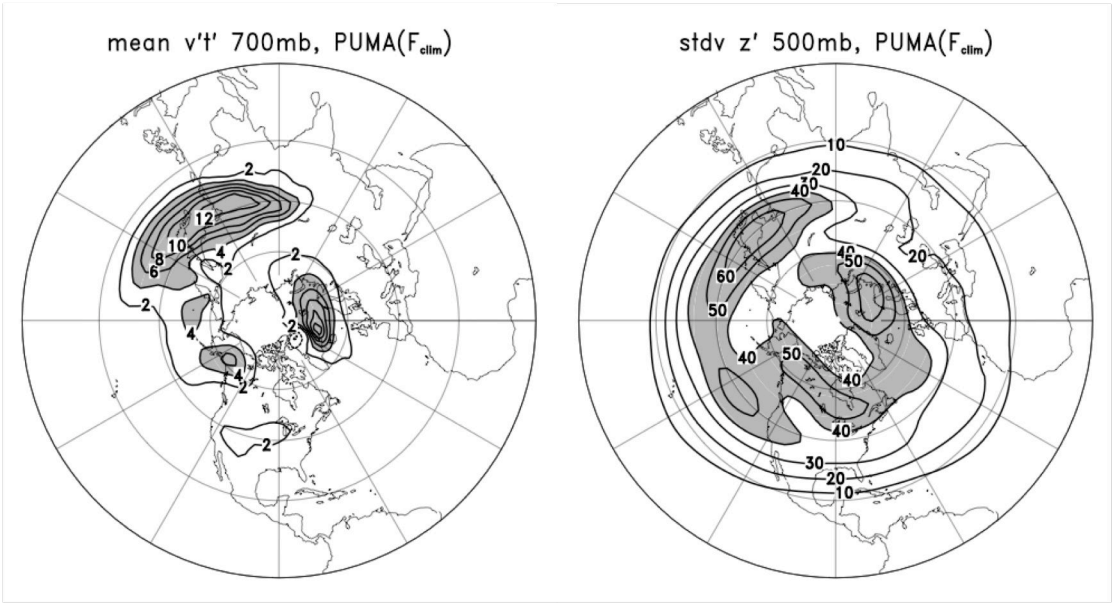

Figure 11. Simulated 700 mb poleward transient-eddy heat flux (left panel; K m/s) and standard deviation of daily 500 mb heights (right panel; m) in a constant forcing simulation in which the forcing is the sum of the mean diabatic forcing and forcing by the mean adiabatic transient-eddy fluxes. These panels should be compared with their counterparts in Fig. 7. Note the smaller contour intervals and smaller values here.